WATER RESOURCES RESEARCH, VOL. 33, NO. 4, PAGES 517–526, APRIL 1997

Experimental investigation of the stability boundary for double-diffusive finger convection in a Hele-Shaw cell

Clay A. Cooper
Desert Research Institute and Hydrologic Sciences Program, University of Nevada, Reno

Robert J. Glass
Subsurface Flow and Transport Processes Laboratory, Sandia National Laboratories, Albuquerque, New Mexico

Scott W. Tyler
Desert Research Institute and Department of Environmental and Resource Sciences, University of Nevada, Reno

Abstract. Double-diffusive convection may be an important transport phenomenon in subsurface porous media and fractures. The classic linear stability analysis derived for a porous medium with two components stratified such that each affects the vertical density gradient in an opposing manner predicts double-diffusive finger instability to occur when $Rs_1 + Rs_2 \geq Rs_c$, where Rs_1 and Rs_2 are the Rayleigh numbers of the faster and slower diffusing components, respectively, and Rs_c is a critical value dependent upon the boundary conditions ($0 \leq Rs_c \leq 4\pi^2$). For cases where $Rs_c/|Rs_1| \ll 1$, the above result can be simplified to $-R_\rho < 1/\tau$, where R_ρ is the buoyancy ratio of the fluid and τ is the ratio of diffusivities ($0 < \tau < 1$). We experimentally tested the applicability of both stability criteria for situations where a narrow transition zone exists bounded above and below by constant concentrations and within a domain of uniform permeability. Experiments were conducted in a Hele-Shaw cell using a digital imaging technique which provided pixel-scale (~0.2 mm) resolution of the evolving concentration field during convection. Within experimental error, our experiments support both criteria within their predicted ranges of applicability.

Introduction

Double-diffusive convection is a transport phenomenon that can occur in fluid systems containing two components that influence local fluid density. The components typically include heat and dissolved solutes. Such systems are globally stable with respect to density; however, if the components have different diffusivities and make opposing contributions to the vertical density gradient, local buoyant instabilities may result, giving rise to convection. The nature of the convective flow strongly depends on the initial distribution of each component. If the component of lower diffusivity is destabilizing to the density gradient, double-diffusive finger (or stationary) convection may result where convection is driven by long, narrow columns of rising and falling fluid. In the opposite case, where the component of higher diffusivity is destabilizing to the vertical density gradient, instability results in fluid motion that is oscillatory and can lead to well-mixed convecting layers separated by sharp steps in fluid density. For each of these regimes (finger or oscillatory), transport of the components occurs much faster than would be predicted by simple diffusive transport alone [*Turner*, 1979]. Both convective regimes continue as long as the boundary conditions are maintained; both "run down" if the energy supplied from the boundaries is diminished. In each case, the global density of the fluid tends to move toward a more stable configuration, that is, heavier on bottom. The theoretical and experimental aspects of these convective regimes have been extensively reviewed by *Turner* [1979, 1985] with application to current problems in oceanography, geophysics, astrophysics, and metallurgy. A popular review of the finger instability in oceanography (known as "salt fingers") has recently been presented by *Schmitt* [1995].

Double-diffusive convection in the subsurface (both porous and fractured media) has been suggested to be important in the transport of fertilizers and solutes from the land surface [*Green*, 1984], migration of contaminants from landfills [*Green*, 1984], transport of heat and solutes in geothermal reservoirs [*Griffiths*, 1981; *Fournier*, 1990], and the evolution of surface and groundwater associated with saline lakes and playas [*Phillips*, 1991]. Most work in porous media has focused on the development of stability theories for a variety of boundary and initial conditions (see work by *Trevisan and Bejan* [1990] and *Nield and Bejan* [1992] for reviews), while only limited experimental work has been conducted [e.g., *Griffiths*, 1981; *Imhoff and Green*, 1988; *Murray and Chen*, 1989; *Taylor and Veronis*, 1986; *Predtechensky*, 1994]. When double-diffusive convection occurs in the subsurface, it can substantially influence mass transport. The experiments of *Imhoff and Green* [1988] demonstrated solute fluxes to be 2 orders of magnitude greater than what would be expected solely due to molecular diffusion. Therefore it is important to establish the location within parameter space of the boundary between stable diffusion-dominated and unstable convection-dominated transport.

Paper number 96WR03811.
0043-1397/97/96WR-03811$09.00

For the condition of opposing linear component concentration profiles throughout the thickness of the domain, *Nield* [1968] derived the critical condition bounding the occurrence of double-diffusive convection in a homogeneous porous medium using a linear perturbation analysis. While numerical studies by *Chen and Chen* [1993] support Nield's finger stability criterion, we are unaware of any experimental studies that test the theoretically derived critical condition for finger convection in porous media. Even if correct, application of Nield's criterion to many problems of interest in contaminant hydrology is somewhat ambiguous; transitions between waters containing different solutes influencing local density will be nonlinear, and the permeability is almost never homogeneous. However, analysis of Nield's result shows that for much of parameter space, the stability criterion can be simplified and made independent of both the length scale associated with the concentration profile and the permeability. In fact, this simplified criterion is identical for porous and nonporous systems. Removal of dependence on these two parameters (knowledge of which is often highly uncertain in the subsurface) results in a more easily applied but restricted criterion. In this paper we experimentally test the applicability of the full and simplified stability criteria for situations where a narrow transition zone exists within a domain of uniform permeability. Our experiments, conducted in a Hele-Shaw cell, support both criteria within their predicted ranges of applicability.

Theory

The linear perturbation analysis for the double-diffusive problem in porous media was first examined by *Nield* [1968]. He considered a horizontally infinite homogeneous and isotropic three-dimensional porous medium of finite thickness H with two dissolved solutes (or components) stratified with concentration Δc_1 and Δc_2 (where subscript 1 refers to the solute of higher diffusivity and subscript 2 refers to the solute of lower diffusivity). To study only the finger instability, the solutes are initially stratified such that c_1 decreases linearly upward and c_2 increases linearly upward. Fluid density decreases upward so that the system is gravitationally stable, and the Oberbeck-Boussinesq assumptions, which include variations in density only in the gravitational term of the momentum equation, are invoked. This simplification is justified for small changes in fluid density and for resulting motion that is primarily vertical.

The governing, perturbed equations of mass, momentum, and solute balance, with a linearized equation of state, are nondimensionalized by using combinations of the thickness of the porous medium (H), maximum concentration difference of each component (Δc_i), and diffusivities of the two components (D_i) to scale the variables. The scaled equations reveal the important dimensionless parameters on which system stability depends: the diffusivity ratio (τ), the buoyancy ratio (R_ρ), and the solutal Rayleigh number (Rs_i) [*Wooding*, 1960] for each ith component:

$$\tau = \frac{D_2}{D_1} \tag{1a}$$

$$R_\rho = \frac{\beta_1 \Delta c_1}{\beta_2 \Delta c_2} \tag{1b}$$

$$Rs_i = \frac{\beta_i \Delta c_i g k H}{D_i \nu}. \tag{1c}$$

Here β_i is the volumetric expansion coefficient, g is acceleration due to gravity, k is intrinsic permeability, and ν is the kinematic viscosity of the solution. For the case where one of the components is heat, a thermal Rayleigh number is used, with β_1, Δc_1, and D_1 replaced by the thermal expansivity, change in temperature, and thermal diffusivity, respectively.

The linearized perturbation equations are solved using a normal mode analysis, which results in an eigenvalue problem. *Nield* [1968] solved the eigenvalue problem for various combinations of boundary conditions. He found that the finger instability can only occur when the sum of the solutal Rayleigh numbers exceeds a critical value, that is,

$$Rs_1 + Rs_2 \geq Rs_c \tag{2}$$

where $0 \leq Rs_c \leq 4\pi^2$, depending upon the upper and lower boundary conditions. For example, two impermeable constant-concentration boundaries yield $Rs_c = 4\pi^2$. Figure 1 is a stability plot in solutal Rayleigh number space that shows the location of the possible types of transport phenomena, as determined by *Nield* [1968] and *Nield and Bejan* [1992], for double-diffusive transport in a horizontally infinite porous medium bounded above and below by two impermeable planes of constant solute concentration. Shown are the finger and oscillatory unstable (convective) regions and the stable (diffusive) region. As the upper and lower boundary conditions are relaxed, Rs_c is reduced until it becomes zero for constant pressure and constant solute flux on both boundaries. This reduction results in a slight expansion of the zone of instability within parameter space.

The influence of k and H can be consolidated into a single term by writing (2) in terms of the buoyancy ratio and the ratio of the diffusivities:

$$\left(\frac{Rs_c}{Rs_1} - 1\right) R_\rho \leq \tau^{-1}. \tag{3}$$

Figure 2 shows the stability regime governed by (3) as a function of Rs_1 and ratio of solute diffusivities. Three values of diffusivity ratio are shown (0.2, 0.352, and 0.5); these are representative of typical diffusivity ratios of naturally occurring solutes. (Note that for the case where one of the components is heat, the value of τ is approximately 0.01.) For large values of $|Rs_1|$ relative to Rs_c, the first term in the parentheses in (3) is negligible and stability is primarily governed by R_ρ. For example, Figure 2 suggests that when $\tau = 0.352$, the stability regime is primarily governed by the buoyancy ratio whenever Rs_1 is less than approximately -300. Thus for much of parameter space, (3) can be reduced to

$$-R_\rho \leq \tau^{-1} \tag{4}$$

and the dependence of system stability on either k or H is removed. While (4) should hold for "large" absolute values of Rs_1 irrespective of the boundary conditions, it is exact for all Rs_1 when constant pressure and constant solute flux on both upper and lower boundaries are imposed. An identical inequality to (4) is found for pure fluid (nonporous) systems under the conditions of negligible $Rs_c/|Rs_1|$ (where Rs_i is defined with k replaced by H^2).

Inequalities (2) and (4) are derived for initial concentration profiles that vary linearly with depth. However, in many subsurface environments, vertical concentration profiles evolve that contain transition zones of variable thickness. For these conditions we consider the application of *Nield*'s [1968] result

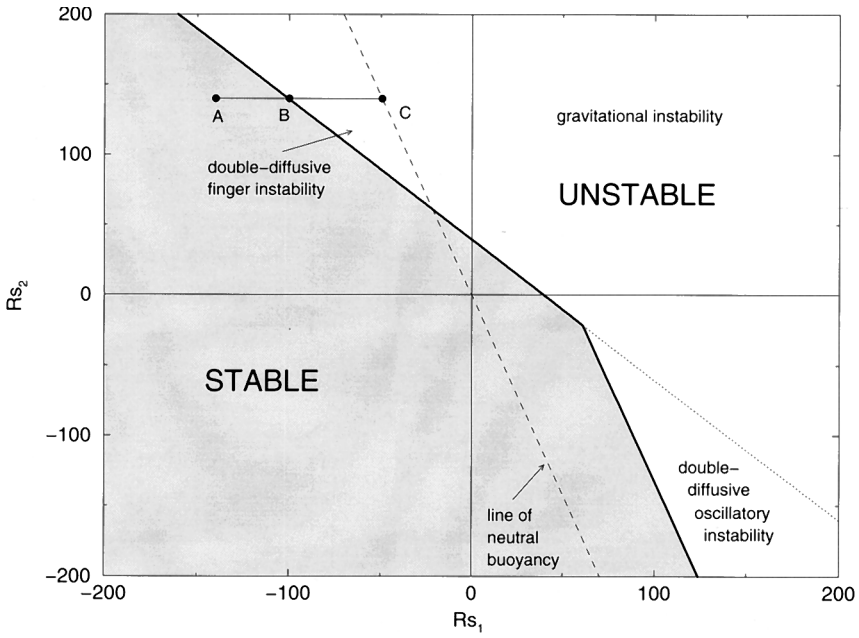

Figure 1. Stability plot in solutal Rayleigh number space that shows the location of the possible types of transport phenomena, as determined by *Nield* [1968] and *Nield and Bejan* [1992], for double-diffusive transport in a horizontally infinite porous medium bounded by two impermeable boundaries of constant solute concentration. The shaded and unshaded areas denote regions of hydrodynamic stability and instability, respectively. For a given porous medium and $\beta_2 \Delta c_2$, point A on the dotted line exists in a stable region, and transport occurs by diffusion alone. An increase in $\beta_1 \Delta c_1$ leads to double-diffusive finger convection initiating at point B. Further increase within the double-diffusive convection regime past C causes the fluid to reach neutral buoyancy, resulting in motion that is probably driven by both density and double-diffusive instabilities, until at $\beta_1 \Delta c_1 = 0$, only one solute is present, and *Horton and Rogers*' [1945] and *Lapwood*'s [1948] criterion for density-driven convection is reached ($Rs_2 \geq 4\pi^2$). As $\beta_1 \Delta c_1$ is increased from zero, both solutes are destabilizing, no double-diffusive motions can occur, and transport is driven by the positive upward density gradient of both solutions. Oscillatory convection occurs in the fourth quadrant (Rs_1 positive and Rs_2 negative); at large absolute values of Rs_1 and Rs_2, the transition from oscillatory to a direct instability mode is, however, no longer defined by (2) [*Baines and Gill*, 1969].

by replacing H with a local length scale, l, defined by the thickness of the transition zone over which the concentration profile is approximately linear. Taking the boundary conditions at the top and bottom of the transition zone as nearly constant pressure and concentration, the critical condition is $Rs_c = 12$ [*Nield*, 1968; *Nield and Bejan*, 1992]. As seen in (3), a lower value of Rs_c results in an increase within parameter space of the range of applicability of (4); once again, for $Rs_c/|Rs_1| \ll 1$, the stability boundary for double-diffusive fingering is independent of l, k, and the boundary conditions.

Experimental Design

A set of experiments was designed to test the stability criteria (2) and (4) applied to systems containing a transition zone of variable thickness l within a domain of height H such that $l \ll H$. Critical to our experimental design was the actual measurement of l within each experiment. Therefore experiments were conducted in a Hele-Shaw cell, where high-resolution digital imaging techniques could be applied and l could be measured.

Experimental Apparatus and Procedure

The Hele-Shaw cell used in our experiments consisted of two rectangular 13-mm-thick clear acrylic plates separated by a thin shim along the cell perimeter. The inner dimensions of the cell were 310 × 170 mm. The cell spacing, b, varied from 0.495 to 0.515 mm (measured volumetrically) depending on the experiment (the cell was disassembled several times for cleaning). The upper and lower regions of the cell were divided by milling a narrow groove (1.0 mm deep × 0.4 mm wide) horizontally across the center on the inside of each plate. Once the two plates were bolted together, a thin Mylar® slider could be moved into or out of the groove to allow separate filling of the cell with the two solutions. The lower horizontal boundary and the two vertical side boundaries of the cell were impermeable to flow. The upper horizontal boundary contained two small openings across the top that allowed air to escape as the cell was filled.

The cell was clamped onto the face of a test stand that allowed cell inclination to vary from horizontal (0°) to vertical (Figure 3); for our experiments the angle was held constant at 25°, which reduced gk in (1c) to gk sin (25°). The test stand contained a bank of high-frequency (40 kHz) fluorescent lamps that were electronically controlled with a feedback loop to minimize light intensity changes throughout the course of an experiment. A light diffuser plate was placed between the light bank and Hele-Shaw cell to uniformly backlight the transparent cell. A Photometrics® charge-coupled device (CCD) camera (2048 × 2048 pixels; 4096 gray levels) mounted above the cell recorded images of the entire flow field at a pixel density

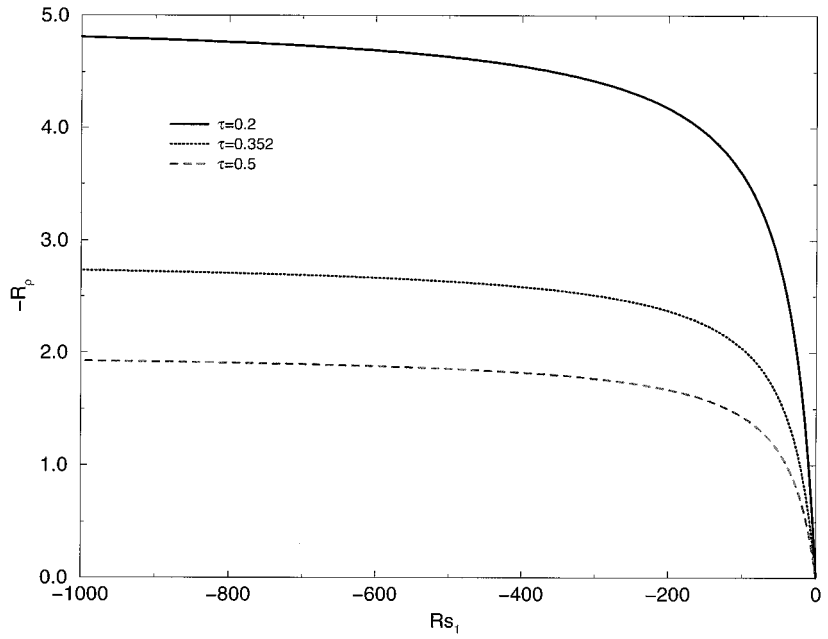

Figure 2. Buoyancy ratio (plotted as $-R_\rho$) as a function of solutal Rayleigh number of the faster diffusing solute (Rs_1) for various diffusivity ratios (τ). The experiments conducted in this study were carried out with sodium chloride as the faster diffusing solute and sucrose as the slower diffusing solute ($\tau = 0.352$). The range of influence of Rs_1 increases with decreasing τ.

of 5.5 pixels mm^{-2}. To visualize convection, a small amount of blue dye (0.0005 kg dye/kg water or less; FD&C blue #1 in all experiments) was added to one of the two solutions and a red filter was attached to the CCD camera. The dye concentration field is used as a surrogate to track the solute concentration with which it was originally mixed. Once the instability began, transport due to convection dominated diffusion, thus giving confidence that the dye concentration mapped the concentration of the corresponding solute. Further details of this light transmission digital image measurement system applied to a variety of experimental systems can be found in work by *Glass and Nicholl* [1995], *Nicholl and Glass* [1994], *Norton and Glass* [1993], and *Tidwell and Glass* [1994].

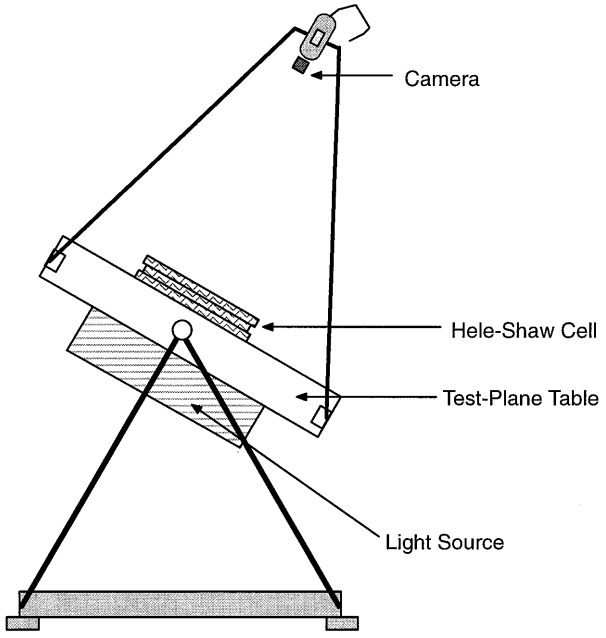

Figure 3. Experimental apparatus showing Hele-Shaw cell on the rotating test stand.

In all experiments a solution of sodium chloride (NaCl) was overlain by a solution of sucrose. Immediately preceding each experiment, the bottom half of the Hele-Shaw cell was filled with a NaCl solution ($\Delta c_1 = 0.01088$ kg NaCl/kg water), which was the same for all experiments. The plastic slider was inserted across the cell through the grooved slot. The top half of the cell was then filled with a sucrose solution. The initial sucrose concentration (Δc_2), and thus the initial buoyancy ratio (R_ρ), was systematically varied in the experimental series from 0.0064 to 0.01381 kg sucrose/kg water to approach the point of critical stability. Each experiment began by slowly removing the slider from the cell, which created a transition zone of thickness l that varied across the width of the cell. The variable l resulted in a range of local Rayleigh numbers represented across the transition zone within a single experiment. Digital images were recorded throughout each experiment at intervals from 1 minute to four hours. The duration of each experiment ranged from 40 to 100 hours; 12 experiments were conducted in the set (see Tables 1 and 2).

Digital Image Reduction

Each image was first processed to remove lighting and CCD sensor array variation through calculation of a normalized image. The normalized gray level of an individual pixel within a normalized image, I_n, is given by

$$I_n = \frac{I_i - I_{\text{cl}}}{I_{\text{dye}} - I_{\text{cl}}} \tag{5}$$

where I_i, I_{cl}, and I_{dye} are the gray levels of individual pixels in the image being normalized, a clear (zero kilograms of dye per kilogram of water) reference image, and a dyed reference

Table 1. Initial Conditions and Result for Each Experiment

Experiment	$k \times 10^8$, m^2	Δc_2	l_{ave},* mm	Rs_1	Rs_2	$-R_\rho$†
			Unstable Experiments			
1‡	2.21	0.01381	3.3	−1549	3067	1.43
2§	2.14	0.01381	5.1	−2318	4591	1.43
3‡	2.21	0.01088	2.4	−1126	1758	1.82
4§	2.14	0.01088	9.3	−4226	6595	1.82
5‡	2.21	0.00826	5.9	−2769	3280	2.40
6‖	2.21	0.00826	4.2	−1971	2335	2.40
7‖	2.19	0.00750	11.1	−5162	5553	2.64
8‖	2.19	0.00740	9.9	−4604	4887	2.67
9§	2.14	0.00740	4.4	−1999	2122	2.67
10§	2.14	0.00710	4.4	−1999	2036	2.79
11‖	2.19	0.00690	4.3	−2000	1779	2.87
			Stable Experiment			
12‖	2.19	0.00640	4.6	−2139	1964	3.09

Subscript 1 refers to NaCl solution; subscript 2 refers to sucrose solution. For all experiments, $\Delta c_1 = 0.01088$, $\beta_1 = -0.755$, $\beta_2 = -0.415$, $\theta = 25°$, $\nu = 1.025 \times 10^{-6}$ m^2 s^{-1}, and $g = 9.81$ m s^{-2}.

*The length scale is the thickness of the transition zone at the start of the experiment; standard deviation of l_{ave} estimated as 46% for all experiments.

†Instability predicted by (4) when $-R_\rho < 2.84$.

‡Dye concentration 0.5 g/kg in sucrose.

§Dye concentration 0.125 g/kg in NaCl.

‖Dye concentration 0.125 g/kg in sucrose.

image, respectively. Each I_n image was then used to calculate through a measured calibration curve a relative concentration field (c/c_0), where c_0 is the concentration of solute in the dyed component at the start of an experiment.

Calibration curves were constructed from average light intensity values for the entire cell (new calibration curves were measured each time the cell was disassembled). For example, the curve used in experiments 2, 4, 9, and 10 was developed by recording separate images of the cell filled with a 0.01 kg NaCl/kg water concentration with a range of dye concentrations of 1.25×10^{-4}, 6.25×10^{-5}, 3.125×10^{-5}, 1.5625×10^{-5}, 7.8125×10^{-6} and zero kg dye/kg water. I_i for these images was converted to I_n, and its average value for the entire cell was used to fit a polynomial across the concentrations considered ($R^2 \geq 0.99$ for all curves). The accuracy of this method was checked by tracking the total mass of dyed solute within each image for every experiment. Mass was found to be conserved within 2% even when the concentration field became greatly distorted by convection. It should be noted that the direct application of the Beer-Lambert law for light transmission without the development of a calibration curve did not yield mass balance.

Estimation of Dimensionless Parameters and Their Uncertainties

The diffusivity ratio, τ, was calculated using from *Stokes* [1950] and *Gosting and Morris* [1949] the molecular diffusivities of NaCl (D_1) and sucrose (D_2) as functions of concentration. The values were interpolated to concentrations of 50% of their maximum in each experiment, assumed to be representative of the concentration within the transition zone between the two solutions. The diffusivities were further adjusted for temperature, using the Stokes-Einstein relation [*Gosting and Morris*, 1949]

$$D_T = D_{25} \frac{\nu_{25} T_T}{\nu_T T_{25}} \tag{6}$$

Table 2. Minimum and Maximum Length Scales for Each Experiment and Resulting Solutal Rayleigh Numbers

Experiment	l_{min}, mm	l_{max}, mm	Rs_{1min}	Rs_{1max}	Rs_{2min}	Rs_{2max}
			Unstable Experiments			
1	1.8	4.9	−845	−2300	1673	4555
2	2.0	8.2	−909	−3726	1800	7381
3	1.1	3.8	−516	−1783	806	2783
4	3.7	14.8	−1681	−6725	2624	10495
5	2.2	9.6	−1018	−4505	1206	5337
6	1.5	6.9	−704	−3238	834	3836
7	8.7	13.4	−4050	−6232	4357	6704
8	3.3	16.4	−1539	−7627	1634	8095
9	3.0	5.9	−1363	−2681	1447	2846
10	2.1	6.6	−954	−2999	972	3054
11	3.1	5.4	−1441	−2511	1427	2485
			Stable Experiment			
12	3.3	5.9	−1534	−2744	1409	2519

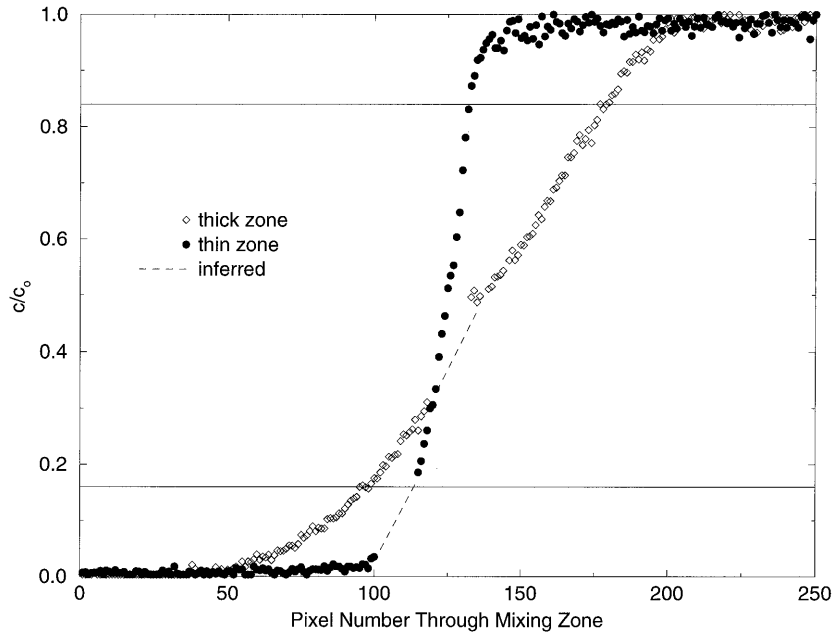

Figure 4. Normalized sodium chloride concentration profiles through the thickest and thinnest vertical sections of the initial mixed layer of experiment 4. The minimum and maximum length scale ($l_{\min}$ and $l_{\max}$) were determined as the distance between 16% and 84% of the normalized NaCl concentration (the horizontal lines) through the thinnest and thickest parts of the mixed layer. The average length scale, l_{ave}, was determined from the average of these two values. The dashed line represents data loss due to the position of the groove the slider.

where T refers to absolute temperature, and subscripts 25 and T refer to properties at 25°C and the temperature of the cell during an experiment. Solute diffusivities for all experiments were adjusted for 27.5°C (the temperature measured in the cell on the test stand) and were calculated as $D_1 = 1.57 \times 10^{-9}$ m^2 s^{-1} and $D_2 = 5.53 \times 10^{-10}$ m^2 s^{-1} (with a standard deviation of ±5%, which included uncertainties in temperature and viscosity). For experiments farther away from the stability boundary, that is, clearly within the region of unstable convection, compensation for temperature had little effect on the instability prediction. The buoyancy ratio, R_ρ, was calculated using volumetric expansion coefficients taken from *Weast* [1977] (standard deviation estimated as ±2%). Assuming a standard deviation in Δc_i of ±1% results in standard deviations in the dimensionless parameters τ and R_ρ of 7% and 3%, respectively.

The solutal Rayleigh number, Rs_i, contains the three additional parameters: viscosity, cell permeability, and length scale over which the concentration varies, l. Values of viscosity as a function of solute concentration were taken from *Weast* [1977] (with standard deviation of ±2%). The cell permeability (b^2/12) was calculated from the parallel plate analogue [*Bear*, 1988] (with standard deviation of ±5%). We took l as the thickness of the mixed layer between the upper and lower solutions where the concentration profiles are primarily linear; l was measured by analyzing the concentration field at the beginning of each experiment. Plate 1 (from experiment 4) shows a typical initial transition zone between the two solutions. The method used to fill the cell and remove the slider created variations in l horizontally across the cell which resulted in a range of initial solutal Rayleigh numbers within this zone for each experiment. The largest and smallest distances encompassing ±1 standard deviation of the concentration profile (i.e., c/c_0 between 0.16 and 0.84, where the concentration gradient is primarily linear) were chosen as a minimum and maximum l, respectively (Figure 4). The arithmetic average of these values (l_{ave}) was taken as a representative value of l for each experiment. As a measure of the uncertainty associated with l_{ave} for an experiment, the variance in l across the width of the cell was calculated for a typical experiment (4, which had average values of R_ρ and l). The standard deviation of this distribution (46%) was assumed for all experiments and overwhelms the contribution of the other terms; therefore the standard deviation in Rs_i for all experiments was taken as 46% (see Tables 1 and 2).

Results

Of the 12 experiments conducted, one experiment (12) displayed stable behavior, while the remaining 11 experiments showed various degrees of instability along some portion of the transition zone. Analysis of images from each unstable experiment taken during the initial development of the instabilities revealed that the fingers formed simultaneously throughout the thickness of the vertical zone encompassed by l. No systematic trend with respect to the location of the first appearance of fingers horizontally across the cell in any single experiment was observed; in some experiments fingers formed first in zones where l was small, while in others they first formed in zones where l was large. However, fingers eventually formed horizontally across the entire transition zone.

The time to the development of instability, defined here as the time when fingers were observed horizontally across 1/4 of the cell, was utilized to help determine the stability threshold. If several hours passed before the instability developed, we knew that the particular experiment was very close to the stability boundary and that the time to instability approached the timescale of the transverse diffusive stabilizing influences.

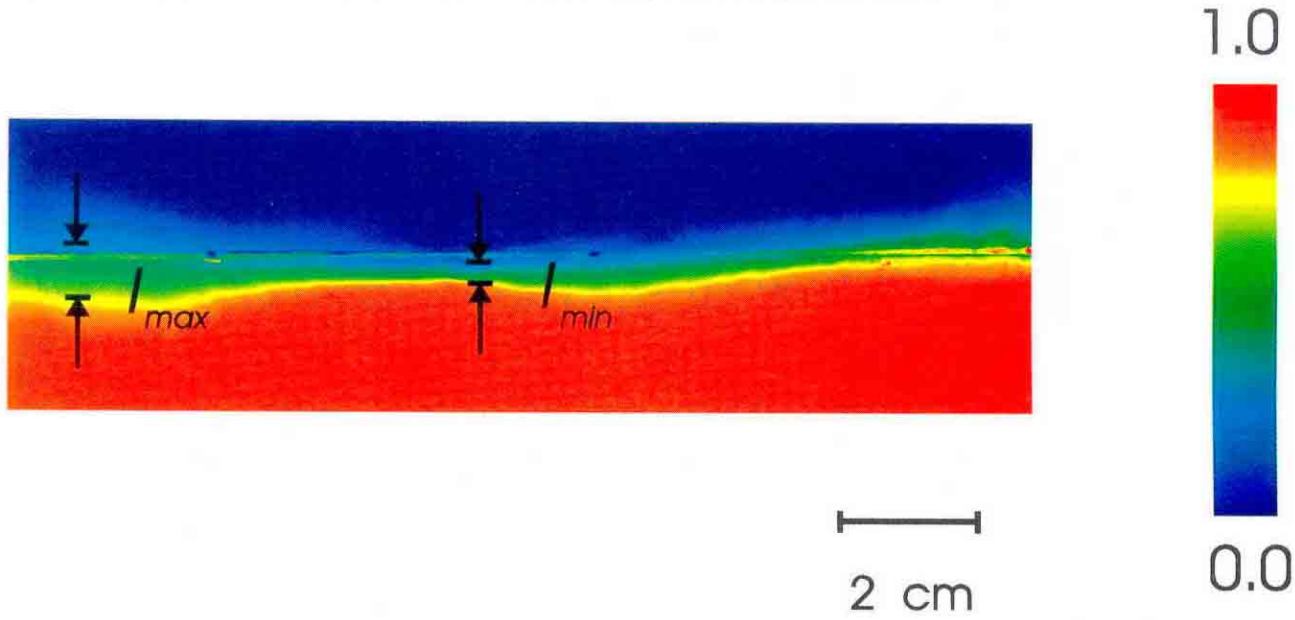

Plate 1. Normalized (c/c_0) sodium chloride concentration of the transition zone at the start of experiment 4. The zone is not level because of disturbances to the interface of the two solutions while filling the top half of the cell and removing the slider separating the two solutions. The image dimensions are approximately 156 × 40 mm.

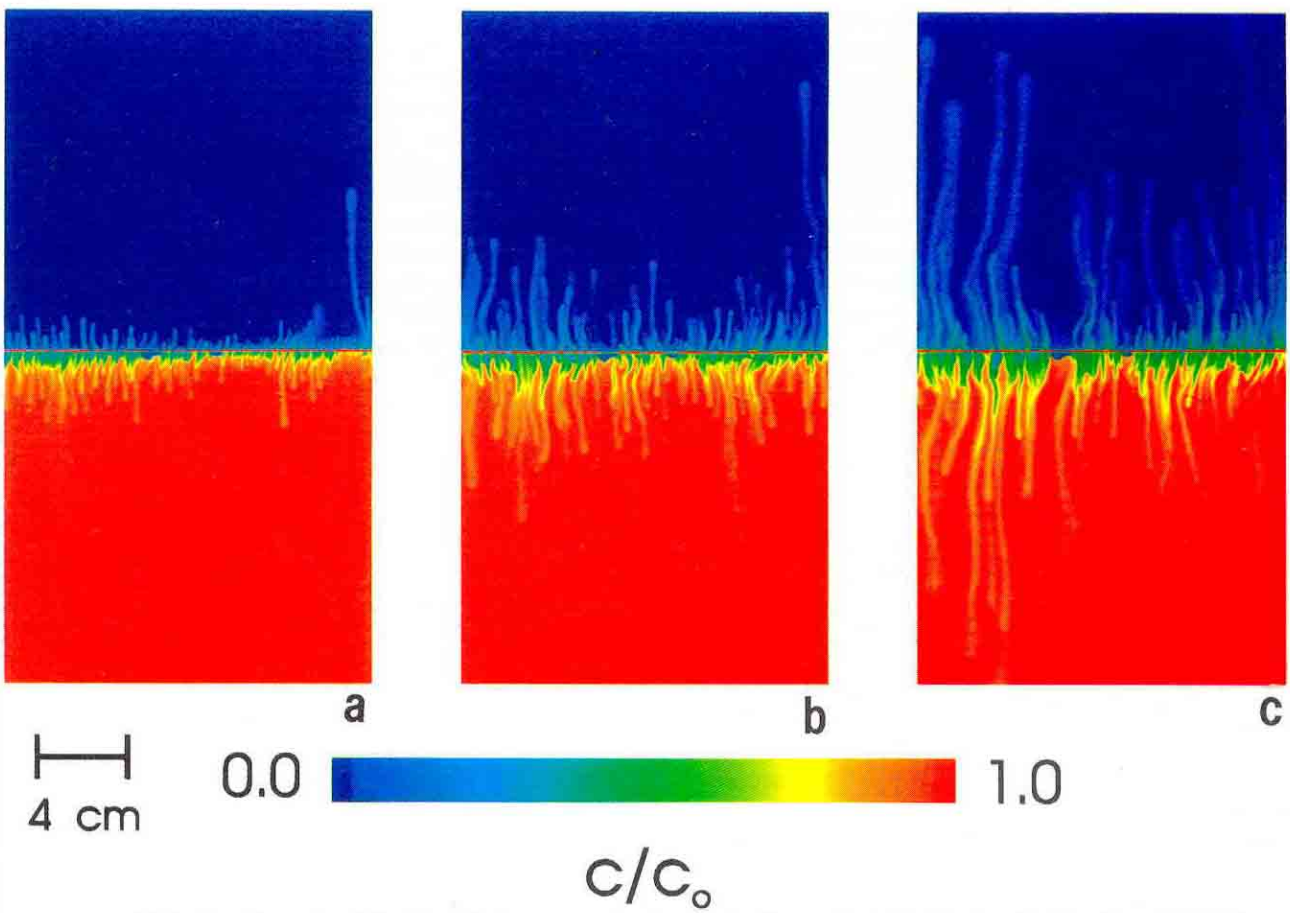

Plate 2. Example of double-diffusive convection in a Hele-Shaw cell at (a) 37 min, (b) 84 min, and (c) 187 min after the start of experiment 2. Upward and downward traveling fingers composed of both NaCl and sucrose form as a result of the development of local buoyant instabilities. The color scale maps the normalized NaCl field, though the sucrose field can also be inferred from the figures.

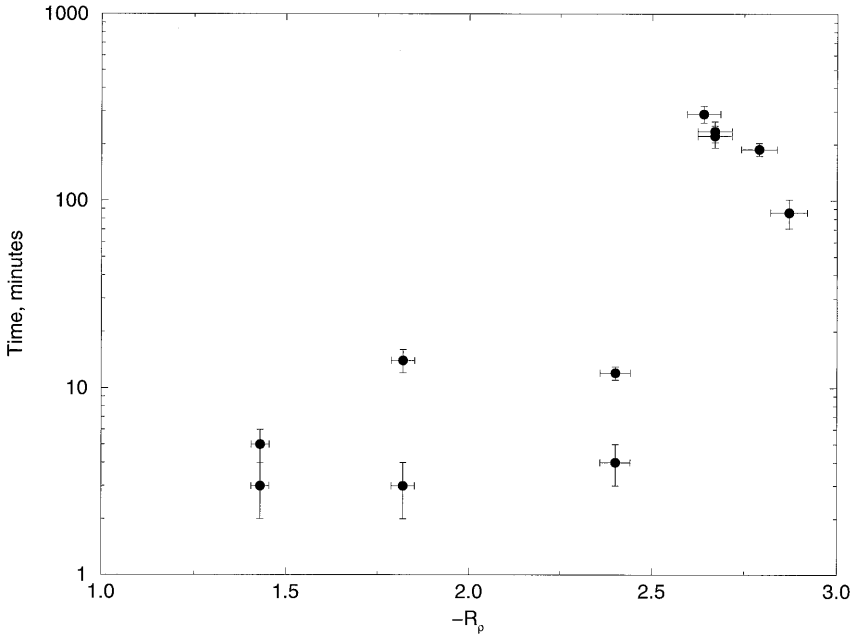

Figure 5. Time to the start of the instability as a function of the initial buoyancy ratio (plotted as $-R_\rho$). The instability takes longer to develop in experiments closer to stable initial conditions. Incipient instability was defined as the formation of fingers across 1/4 of the mixing zone. Error bars shown for ± 1 standard deviation.

Figure 5 shows the time required for instability to develop as a function of $-R_\rho$ for each unstable experiment and shows that as the initial buoyancy ratio approaches stability, significantly more time is required for the instability to develop.

Plates 2a–2c present the NaCl concentration field at three times during one experiment (experiment 2) in which $-R_\rho = 1.43$. Both figures depict fingers of high NaCl concentration traveling upward into the sucrose field, while low NaCl concentration fingers travel downward. Plate 2a shows the development of the instability 37 min after the beginning of the experiment. The largest fingers are 20 to 30 mm long. Fingering development after 84 min is shown in Plate 2b. In several places smaller fingers have coalesced near their base to form fewer larger fingers, while in others, fingertips have split to form separate fingers. Plate 2c shows the fingering development after 187 min. The largest fingers are 120 to 150 mm long and have nearly filled both halves of the cell. Further discussion of the details of unstable flow field evolution and analysis of data to yield cell-scale mass fluxes will be presented elsewhere.

Figure 6 shows the location of each experiment in Rayleigh parameter space, along with the estimated uncertainties for each solutal Rayleigh number. The Rayleigh numbers based upon minimum and maximum length scales ($l_{\min}$ and $l_{\max}$) and average length scale (l_{ave}) are plotted. The large error bars associated with average solutal Rayleigh numbers for each experiment reflect the large variation in the thickness of the initial transition zone between the two solutions. The Rayleigh numbers based on $l_{\min}$ and $l_{\max}$ show much less uncertainty because these reflect single measured values and contain only uncertainties in fluid and cell properties. Also shown is the line of neutral stability ($-R_\rho = 1.0$) and the boundary predicted by *Nield and Bejan* [1992] between stable diffusion and unstable double-diffusive finger convection for our boundary conditions. Uncertainties in l_{ave} make quantitative evaluation of (2) using average solutal Rayleigh numbers difficult. However, the stable experiment plots on the line predicted by (2) for $Rs_c = 12$ and qualitatively confirms stable double diffusion.

In order to investigate the validity of the stability criterion developed in (4), the term $Rs_c/|Rs_1|$ in (3), along with its uncertainty, must be "small" in comparison to unity. For all experiments the value of $Rs_c/|Rs_1|$ (based upon the average length scale) was less than 0.02. Figure 7 gives the results plotted as a function of $-R_\rho$. The stability boundary is predicted from (4) as $-R_\rho = 2.84$. Within the experimental errors identified previously, all unstable experiments plot in the field $0 < -R_\rho < 2.84$ and strongly support the validity of (4).

Figure 7 also shows a theoretical stability criterion developed by *Huppert and Manins* [1973] for a diffusive profile developed across a step transition between two solutions in a nonporous system. Their results extend directly to porous media yielding a similar expression to (4) although with an exponent on τ of $-3/2$. For NaCl and sucrose, Huppert and Manins' result predicts stable fluid motion when $-R_\rho > 4.8$. Our experimental results do not support this criterion; however, our initial condition (a mechanically mixed zone of finite thickness l) was very different from theirs. Huppert and Manins assumed that a diffusive interface initially develops between the two solutions with the different solute diffusivities resulting in solution profiles that are not symmetrical to each other about the original interface. In contrast, our experiments began with a transition zone throughout where both solutes are mechanically mixed, producing an identical l for each solute at the beginning of the experiment.

Our experimental results apply directly to an ideal smooth-walled fracture. However, for convection in a Hele-Shaw cell to be valid in analogy to convection in porous media, three criteria must be satisfied that relate cell gap to the flow dynamics [*Wooding*, 1960]:

$$b \ll \delta \tag{7a}$$

$$Ub^2/D\delta \ll 1 \tag{7b}$$

$$Ub^2/\nu\delta \ll 1 \tag{7c}$$

where δ is the smallest convective length scale of motion and U is the velocity scale. These three inequalities ensure negligible

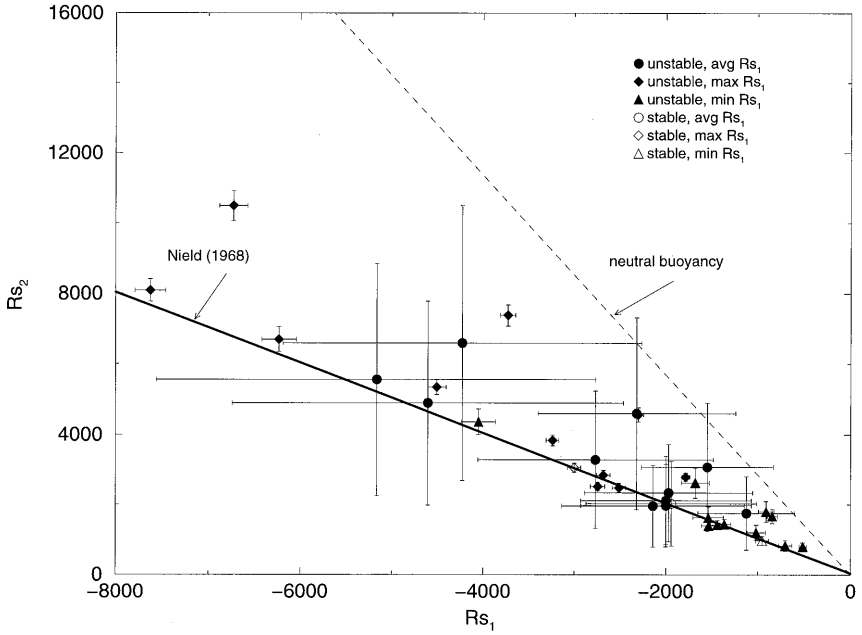

Figure 6. Location of initial conditions for each experiment in solutal Rayleigh number space. Rs_1 and Rs_2 are the solutal Rayleigh numbers for NaCl and sucrose, respectively. Closed symbols represent unstable experiments, and the open symbols represent the experiment that was stable. Data for Rayleigh numbers based upon l_{ave} (circles), $l_{\min}$ (triangles), and $l_{\max}$ (diamonds) are presented. Error bars shown for ± 1 standard deviation.

advection of vorticity, rapid diffusion of mass, and rapid diffusion of momentum, respectively, across the gap. We find from our experiments that as soon as fingers are detectable, (7a)–(7c) are satisfied with measured values for U and δ as represented by either the finger width, finger amplitude, or l. However, at the initial development of the instability (where our study is focused) there is some ambiguity in the determination of δ. Convective velocities grow from values of zero to nonzero with corresponding length scales of motion either fixed (e.g., finger width or transition zone thickness l) or growing from near zero (e.g., initial infinitesimal finger amplitude) to up to the size of the system. Assuming δ as always nonzero and given by the fixed values of finger width or the transition zone thickness (l) that initial fingers span, the criteria given by (7a)–(7c)

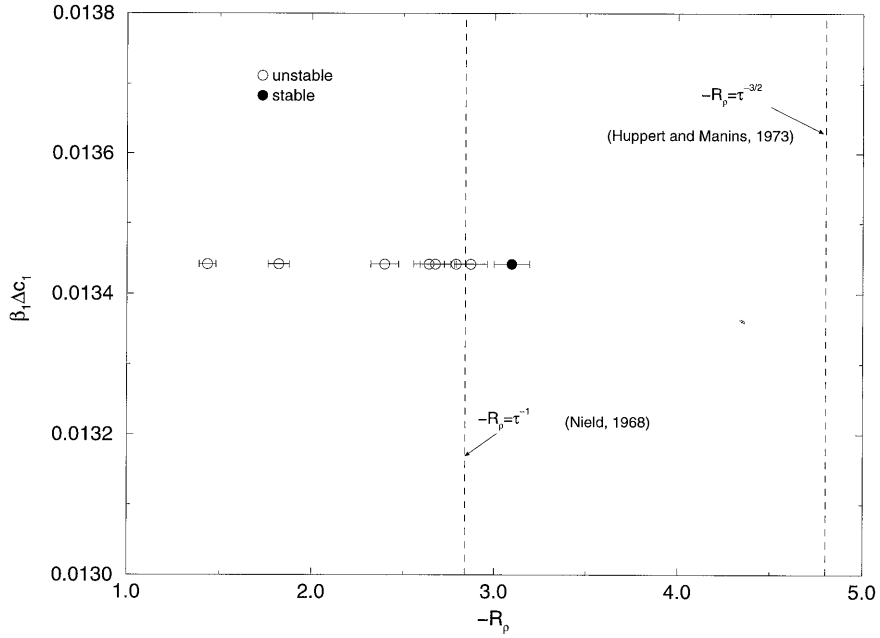

Figure 7. Initial conditions and result of each experiment in the space of $\beta_1 \Delta c_1$ and $-R_\rho$. Open circles represent unstable experiments that resulted in fingering, while the closed circle represents the stable experiment. *Nield*'s [1968] simplified analysis suggests instability for $-R_\rho < 2.84$, while *Huppert and Manins*' [1973] analysis suggests instability for $-R_\rho < 4.8$.

are satisfied by all of our experiments. However, the choice of δ as the infinitesimal amplitude of the initial disturbance dictates that (7a)–(7c) are never satisfied during the initial development of the instability. We believe the most reasonable choice for δ is the finger width, as it is not imposed on the system but develops naturally as the most unstable wavelength within the plane of the Hele-Shaw cell.

Conclusion

While the experimental results reasonably confirm that the stability regime of a laboratory system can be predicted from linear stability analysis, application to natural subsurface environments is more difficult due to uncertainties and variabilities in several of the parameters. The full linear theory first developed by *Nield* [1968] assumes a simple homogeneous and isotropic aquifer with linear concentration profiles and ideal boundary conditions. This contrasts with many subsurface environments composed of three-dimensionally varying permeability and solute concentration fields that are constrained by nonideal boundaries. In addition to these inconsistencies with theoretical assumptions, estimation of subsurface permeabilities and solute transition zone thicknesses is inherently uncertain, making application of (2) to many natural environments even more problematic.

Our results suggest that in the region of parameter space where the buoyancy ratio formulation (4) should apply (i.e., $Rs_c/|Rs_1| \ll 1$), simplification of the full linear theory (2) to (4) may provide a realistic estimate of the stability regime for many subsurface systems provided that rough estimates of the ranges of k and l are available. This greatly simplifies determination of the stability regime, as once it is assured that $Rs_c/|Rs_1| \ll 1$, only information pertaining to the type of dissolved solutes in the porous medium and their concentration differences is required.

The study of double-diffusive convection in porous media continues to suffer from a lack of fundamental experimental work. To accurately assess its role in natural subsurface systems, further experimentation and theoretical development are required to investigate additional complexities such as media heterogeneity and anisotropy, shapes of the initial concentration profiles, influence of a third (or more) density-affecting component (true multicomponent convection), and occurrence of chemical reactions.

Acknowledgments. Financial support for this research was provided by the U.S. Department of Energy under the EPSCoR Traineeship program, Sandia National Laboratories, the Desert Research Institute, and the Department of Energy's Basic Energy Sciences Geoscience Research Program under contract numbers DE-FG03-96ER14611 (Desert Research Institute) and DE-AC04-94AL85000 (Sandia National Laboratories). Experiments were conducted in the Subsurface Flow and Transport Processes Laboratory at Sandia National Laboratories. We thank Mike Nicholl and Dennis Norton for assistance with various aspects of running the experiments and W. Craig Ginn for technical expertise in the fabrication of several test cells. We also thank Harlan Stockman, Mike Nicholl, Jean Bahr, and two anonymous reviewers for their careful reviews and helpful comments.

References

Baines, P. G., and A. E. Gill, On thermohaline convection with linear gradients, *J. Fluid Mech*., *37*, 289–306, 1969.

Bear, J., *Dynamics of Fluids in Porous Media*, 764 pp., Dover, Mineola, N.Y., 1988.

Chen, F., and C. F. Chen, Double-diffusive fingering convection in a porous medium, *Int. J. Heat Mass Transfer*, *36*, 793–807, 1993.

Fournier, R. O., Double-diffusive convection in geothermal systems: The Salton Sea, California, geothermal system as a likely candidate, *Geothermics*, *19*, 481–496, 1990.

Glass, R. J., and M. J. Nicholl, Quantitative visualization of entrapped phase dissolution within a horizontal flowing fracture, *Geophys. Res. Lett*., *22*, 1413–1416, 1995.

Gosting, L. J., and M. S. Morris, Diffusion studies on dilute aqueous sucrose solutions at 1° and 25° with the Gouy interference method, *J. Am. Chem. Soc*., *71*, 1998–2006, 1949.

Green, T., Scales for double-diffusive fingering in porous media, *Water Resour. Res*., *20*, 1225–1229, 1984.

Griffiths, R. W., Layered double-diffusive convection in porous media, *J. Fluid Mech*., *102*, 221–248, 1981.

Horton, C. W., and F. T. Rogers, Convection currents in a porous medium, *J. Appl. Phys*., *16*, 367–370, 1945.

Huppert, H. E., and P. C. Manins, Limiting conditions for salt-fingering at an interface, *Deep Sea Res*., *20*, 315–323, 1973.

Imhoff, P. T., and T. Green, Experimental investigation of double-diffusive groundwater fingers, *J. Fluid Mech*., *188*, 363–382, 1988.

Lapwood, E. R., Convection of a fluid in a porous medium, *Proc. Cambridge Philos. Soc*., *44*, 508–521, 1948.

Murray, B. T., and C. F. Chen, Double-diffusive convection in a porous medium, *J. Fluid Mech*., *201*, 147–166, 1989.

Nicholl, M. J., and R. J. Glass, Wetting phase permeability in a partially saturated horizontal fracture, in *Proceedings of 5th Annual International Conference on High Level Radioactive Waste Management*, pp. 2007–2019, Am. Nucl. Soc., Las Vegas, Nev., 1994.

Nield, D. A., Onset of thermohaline convection in a porous medium, *Water Resour. Res*., *4*, 553–560, 1968.

Nield, D. A., and A. Bejan, *Convection in Porous Media*, 408 pp., Springer-Verlag, New York, 1992.

Norton, D., and R. J. Glass, Full-field dye concentration measurement within saturated/unsaturated thin slabs of porous media, in *Proceedings of 4th Annual International Conference on High Level Radioactive Waste Management*, pp. 1066–1075, Am. Nucl. Soc., Las Vegas, Nev., 1993.

Phillips, O. M., *Flow and Reactions in Permeable Rocks*, 285 pp., Cambridge Univ. Press, New York, 1991.

Predtechensky, A. A., W. D. McCormick, J. B. Swift, A. G. Rossberg, and H. L. Swinney, Traveling wave instability in sustained double-diffusive convection, *Phys. Fluids*, *6*, 3923–3935, 1994.

Schmitt, R. W., The ocean's salt fingers, *Sci. Am*., *272*, 70–75, 1995.

Stokes, R. H., The diffusion coefficients of eight univalent electrolytes in aqueous solution at 25°, *J. Am. Chem. Soc*., *72*, 2243–2247, 1950.

Taylor, J., and G. Veronis, Experiments on salt fingers in a Hele Shaw cell, *Science*, *231*, 39–41, 1986.

Tidwell, V. C., and R. J. Glass, X ray and visible light transmission for laboratory measurement of two-dimensional saturation fields in thin-slab systems, *Water Resour. Res*., *30*, 2873–2882, 1994.

Trevisan, O. V., and A. Bejan, Combined heat and mass transfer by natural convection in a porous medium, *Adv. Heat Transfer*, *20*, 315–352, 1990.

Turner, J. S., *Buoyancy Effects in Fluids*, 368 pp., Cambridge Univ. Press, New York, 1979.

Turner, J. S., Multicomponent convection, *Ann. Rev. Fluid Mech*., *17*, 11–44, 1985.

Weast, R. C. (Ed.), *CRC Handbook of Chemistry and Physics*, 57th ed., CRC Press, Boca Raton, Fla., 1977.

Wooding, R. A., Instability of a viscous liquid of variable density in a vertical Hele-Shaw cell, *J. Fluid Mech*., *7*, 501–515, 1960.

C. A. Cooper, Hydrologic Sciences Program and Desert Research Institute, University of Nevada, P.O. Box 60220, Reno, NV 89506. (e-mail: clay@maxey.dri.edu)

R. J. Glass, Subsurface Flow and Transport Processes Laboratory, Sandia National Laboratories, M. S. 1324, P.O. Box 5800, Albuquerque, NM 87185-1324. (e-mail: rjglass@sandia.gov)

S. W. Tyler, Desert Research Institute and Department of Environmental and Resource Sciences, University of Nevada, P.O. Box 60220, Reno, NV 89506. (e-mail: scott@maxey.dri.edu)

(Received December 7, 1995; revised December 1, 1996; accepted December 10, 1996.)